



Cite this: *Chem. Sci.*, 2025, **16**, 15518

All publication charges for this article have been paid for by the Royal Society of Chemistry

Single solvent molecule effect over S_N2 and E2 competition in the hydroperoxide anion reaction with ethyl-iodide[†]

Xiangyu Wu, ^a Chongqin Zhu, ^b Joseph S. Francisco ^{*c} and Jing Xie ^{*a}

The influence of individual solvent molecules on the dynamics of competing reactions remains largely unexplored for many important chemical systems. Herein, direct dynamics simulations revealed that a single water molecule has multifaceted effects on the reaction between the hydroperoxide anion HOO^- and $\text{C}_2\text{H}_5\text{I}$. The introduction of one water reduced the overall reaction rate and shifted the preference from elimination (E2) to substitution (S_N2) reactions because of the differential solvation effect. Increasing the collision energy lowered the overall reactivity but did not change the S_N2 -to-E2 pathway ratio. Notably, the additional water molecules also induced new competing pathways that used HO^- as an attacking nucleophile *via* proton transfer within the nucleophile $\text{HOO}^-(\text{H}_2\text{O})$; here, both the HO^- -E2 and HO^- - S_N2 trajectories were observed at small percentages. The occurrence of the HO^- paths was driven by the extensive proton transfer within the pre-reaction complex well, but was suppressed by the entropy effect and increased barriers. In addition, water molecules complicated the reaction mechanisms, increased the percentage of indirect mechanisms, and affected the dynamic features of proton transfer. As in the solvent-free system, protons were frequently exchanged between the nucleophiles and substrates, whereas in the singly solvated system, proton exchange mainly occurred within the nucleophiles. This work highlights the dynamic role of solvent molecules and may have profound impacts on reaction dynamics, with relevance to organic synthesis and chemistry in biosystems, microdroplets, and aerosols.

Received 12th June 2025

Accepted 23rd July 2025

DOI: 10.1039/d5sc04298d

rsc.li/chemical-science

Introduction

In addition to providing a liquid-phase reaction environment, solvents have a profound impact on chemical reactions, such as affecting the reaction kinetics through catalysis^{1–5} or inhibition,⁶ altering the product branching ratios,^{7–9} and modifying

the reaction dynamics.^{4,10,11} The influence of the individual solvent molecules on the reaction dynamics has long been a central topic among experimental and theoretical researchers in the fields of atmospheric, physical, and interfacial chemistry.^{1,3,6,7,9,12–19} In particular, the development of crossed-beam imaging experimental techniques and computational simulation powers enables a detailed investigation of the reaction mechanisms and dynamics.^{10,20–29} Ion–molecule reactions represent a prevalent category of chemical reactions and can potentially be affected by solvent effects.^{10,30–32} However, the dynamic and steric effects caused by the individual solvent molecules remain elusive for numerous critical ion–molecule reactions.

The hydroperoxide anion (HOO^-), which is the conjugate base of hydrogen peroxide (HOOH), is an important species across diverse fields. For example, in atmospheric chemistry, HOO^- participates in reactions that contribute to acid rain formation and ozone consumption.³³ In the cellular biology field, HOO^- is involved in the oxidative processes linked to ageing and degenerative diseases since it reacts with lipids and proteins.^{34–37} Industrially, HOO^- serves as a key oxidant in semiconductor cleaning processes and peroxide bleaching, where it facilitates the breakdown of chromophores to decolorize fabrics.^{38–40} Additionally, HOO^- likely participates in

^aKey Laboratory of Cluster Science of Ministry of Education, School of Chemistry and Chemical Engineering, Beijing Institute of Technology, Beijing 100081, China. E-mail: jingxie@bit.edu.cn

^bKey Laboratory of Theoretical and Computational Photochemistry, Ministry of Education, College of Chemistry, Beijing Normal University, Beijing 100875, China

^cDepartment of Earth and Environmental Science and Department of Chemistry, University of Pennsylvania, Philadelphia, Pennsylvania 19104, USA. E-mail: fjoseph@sas.upenn.edu

[†] Electronic supplementary information (ESI) available: Direct rebound mechanism of the HOO^- - S_N2 path (Video S1); direct stripping mechanism of the HOO^- - S_N2 path (Video S2); direct rebound mechanism of the HOO^- -E2 path (Video S3); direct stripping mechanism of the HOO^- -E2 path (Video S4); indirect mechanism, roundabout mechanism of the HOO^- - S_N2 path (Video S5); indirect mechanism of the H-exchange of the HOO^- - S_N2 path (Video S6); indirect mechanism of the HOO^- -anti-E2 path (Video S7); indirect mechanism of the HOO^- -syn-E2 path (Video S8); indirect mechanism of the α -elimination of the HOO^- -E2 path (Video S9); indirect mechanism of the HO^- - S_N2 path (Video S10); indirect mechanism of the HO^- -E2 path (Video S11). See DOI: <https://doi.org/10.1039/d5sc04298d>



hydrocarbon oxidation and combustion processes, such as acetylene combustion; here, it reacts with formaldehyde and formic acid.^{41,42} Recent advancements in energy storage have also highlighted its importance since shifting the discharge intermediate from superoxide O_2^- to HOO^- in aprotic Li–O₂ batteries can reduce the byproducts and overpotentials to enhance battery efficiency.⁴³ Due to its multifaceted roles, HOO^- needs to be comprehensively understood to advance research in atmospheric science, biochemistry, industrial application, and energy technologies.

The hydrated HOO^- ion has garnered great interest for its unique properties.^{44–49} Microhydrated HOO^- ions, $HOO^-(H_2O)_n$, can undergo proton transfer to generate isomers in the form of $HO^-(HOOH)(H_2O)_{n-1}$, where the latter is lower in energy when the number of water molecules n is less than 6.⁴⁸ Hence, when hydrated HOO^- ions interact with a substrate, they can behave as dual nucleophiles, similar to CN^- , such that either HOO^- or HO^- can act as nucleophiles.^{50–53} Previously, direct dynamics simulations of singly hydrated HOO^- reacting with CH_3Cl and CH_3I revealed that the HOO^- path is dominant and produces CH_3OOH , whereas the HO^- path contributes only a minor fraction of the products and produces CH_3OH .^{32,54} Calculations have shown that increasing the degree of hydration causes the HO^- path to be even less favourable.⁵⁵ Enlarging the substrate from methyl halides to ethyl halides introduces a competing reaction to the S_N2 pathway, namely, elimination reactions (E2).^{4,9,56–58} Either HOO^- or HO^- can serve as the base for the E2 reaction. Interestingly, when singly hydrated HOO^- reacts with ethyl halides, the E2 reaction products of the HOO^- and HO^- paths are identical (Scheme 1) and have similar barriers.⁵⁹ Distinguishing these two product channels by experiment is a formidable task. Therefore, the reaction dynamics need to be investigated using computational simulations.

In this work, we performed direct dynamics simulations on CH_3CH_2I reacting with HOO^- and $HO^-(HOOH)$ in the gas phase to reveal the role of a single water molecule in the reaction dynamics. The key questions we explored are as follows: What is the effect of one water molecule on (1) the reaction kinetics, *i.e.*, the rate constants; (2) the competition between S_N2 and E2 reactions, *i.e.*, their ratio and atomic-level mechanism; and (3) the competition between the HOO^- and HO^- pathways? (4) What is the role of collision energy? The simulations focus on the microhydrated HOO^- ions and reveal that the solvent molecules not only affect the competition between the different

pathways but also influence the dynamic behaviour of chemical reactions. These findings provide valuable theoretical guidance for the environment, energy, and synthesis chemistry.

Computational methods

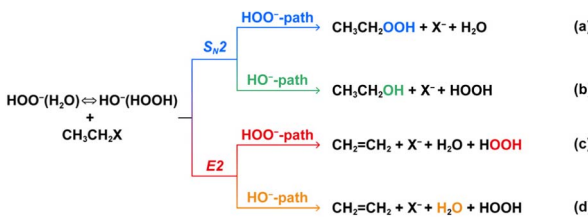
Direct dynamics simulations were performed at the CAM-B3LYP/6-31+G(d,p)&ECP level of theory using the VENUS/NWChem program.^{60–62} The 6-31+G(d,p) basis set was used for the H, C, and O atoms, and the LANL2DZdp basis set and effective core potential (ECP) were used for iodine. The choice of this method was based on the accuracy of the structure and reaction enthalpy (ESI Note and Tables S1–S3†). The initial distance between CH_3CH_2I and HOO^- or $HO^-(HOOH)$ was 15 Å, and the collision energy (E_{coll}) was 0.04 eV (equivalent to 300 K) and 1.0 eV. The vibrational and rotational temperatures of the reactants were 300 K, and the vibrational and rotational energies were sampled for their respective Boltzmann distributions. At an E_{coll} of 0.04 eV, the trajectories were calculated at a fixed impact parameter b of 0, 1, 3, 5, 7, 9, 11, 13, and 15 Å; here, the reaction probability was zero at the maximum b under investigation, namely, b_{max} . At E_{coll} = 1.0 eV, the impact parameter b was 0, 1, 3, 5, 7, and 9 Å for the HOO^- system, and b was 0, 1, 3, 5, and 7 Å for the $HO^-(HOOH)$ system. For each b , approximately 100–120 trajectories were simulated, resulting in a total of 3178 trajectories. Considering the computational efficiency, the trajectories were integrated by the velocity Verlet method⁶³ with a 1.0 fs time step.

Results and discussion

Overall reactivity

The reactivities of CH_3CH_2I with HOO^- and $HO^-(HOOH)$ at collision energies of 0.04 eV and 1.0 eV were evaluated by plotting the opacity functions $P_r(b)$ versus the impact parameter b for the total reaction and different product channels, *i.e.*, the HOO^- - S_N2 , HO^- - S_N2 , HOO^- -E2, and HO^- -E2 pathways (Fig. 1). In comparison, increasing the collision energy decreases both the maximum impact parameter b_{max} and the reaction probability at each b , *i.e.*, $P_r(b)$, which together lower the overall reactivity. For example, for the unsolvated $HOO^- + CH_3CH_2I$ reaction, the value of b_{max} decreases from 15.0 Å at an E_{coll} of 0.04 eV to 9 Å at 1.0 eV; $P_r(b)$ at $b = 1$ Å decreases from 0.89 at 0.04 eV to 0.23 at 1.0 eV. Evaluating the total integral cross sections (ICSSs) σ_r via the formula $\int_0^{b_{max}} P_r(b) 2\pi b db$ provides an σ_r value of $452.8 \pm 7.6 \text{ \AA}^2$ at 0.04 eV and a much smaller value of $17.7 \pm 1.9 \text{ \AA}^2$ at 1.0 eV. The corresponding reaction rate constants of $k(E_{coll}, T_v, T_r) = v(E_{coll})\sigma(E_{coll}, T_v, T_r)$ are (23.8 ± 0.4) and $(4.7 \pm 0.5) \times 10^{-10} \text{ cm}^3 \text{ mol}^{-1} \text{ s}^{-1}$. These results indicate that increasing E_{coll} from 0.04 to 1.0 eV reduces the rate constant by a factor of 4.

Adding one water molecule to the nucleophile barely affects the value of b_{max} but lowers $P_r(b)$. For example, at $b = 1.0$ Å and $E_{coll} = 0.04$ eV, the total $P_r(b)$ decreases from 0.89 for the unsolvated system to 0.49 for the singly solvated system. As a result, this leads to a decrease in the cross-section and



Scheme 1 S_N2 and E2 reaction pathways of the $HOO^-(H_2O) + CH_3CH_2X$ reactions.

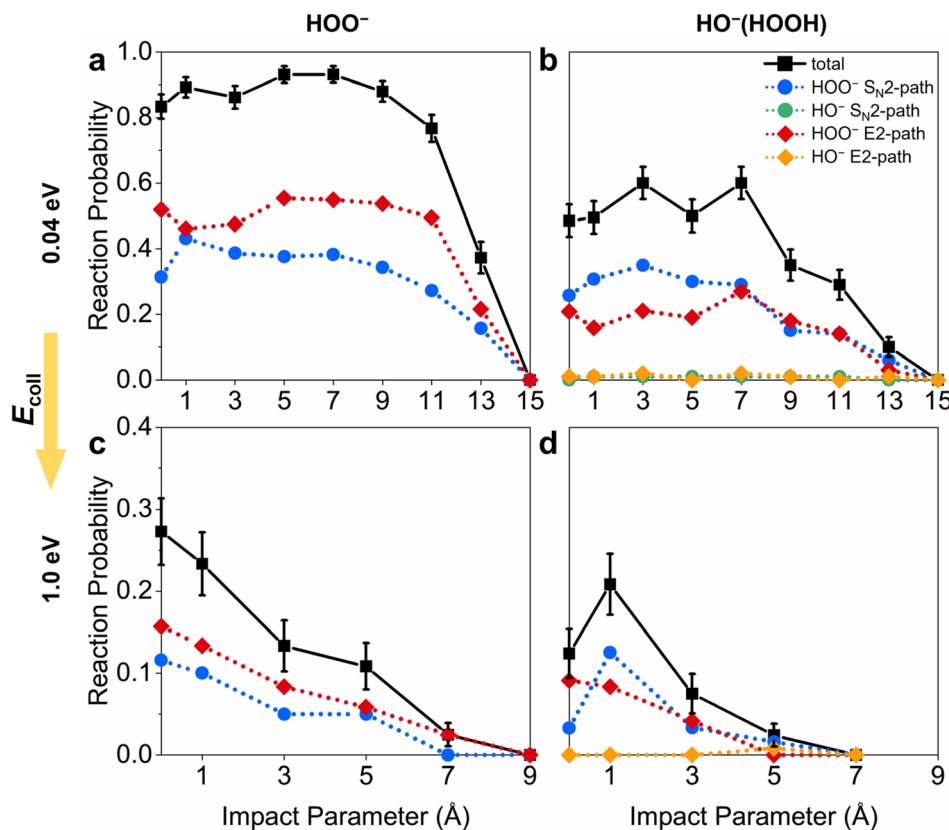


Fig. 1 Opacity functions $P_r(b)$ of the different pathways for $\text{CH}_3\text{CH}_2\text{I}$ reacting with (a and c) HOO^- and (b and d) $\text{HO}^-(\text{HOOH})$ at collision energies of 0.04 eV (top) and 1.0 eV (bottom).

reaction rate constant. For the singly solvated $\text{HO}^-(\text{HOOH}) + \text{CH}_3\text{CH}_2\text{I}$ system, σ_r is $209.2 \pm 8.0 \text{ \AA}^2$ at 0.04 eV and $7.5 \pm 1.0 \text{ \AA}^2$ at 1.0 eV, and the respective rate constants k are (9.3 ± 0.4) and $(1.7 \pm 0.2) \times 10^{-10} \text{ cm}^3 \text{ mol}^{-1} \text{ s}^{-1}$. Taken together, adding one water to the system decreases the rate constant by factors of 1.6 and 1.8 at E_{coll} of 0.04 and 1.0 eV, respectively.

Product channels

The S_{N2} and E2 reactions compete with each other during the reaction process. For the unsolvated system, both the HOO^- -S_{N2} and the HOO^- -E2 pathways occur throughout the range of b from 0 to b_{max} . Notably, the E2 pathway remains dominant over the S_{N2} pathway at each b (Fig. 1a and c). The branching ratio derived from the ICSs for E2 : S_{N2} is 60.4 : 39.6 at 0.04 eV and 62.7 : 37.3 at 1.0 eV (Fig. 2a and c). These results show that increasing E_{coll} slightly enhances the advantage of E2 over S_{N2} reactions, even though the overall reactivity is reduced.

The addition of one water molecule to the system introduces significant changes in the products and their ratios, in addition to affecting the reactivity. At an E_{coll} of 0.04 eV, in addition to the normal HOO^- -S_{N2} and E2 pathways, additional pathways are observed owing to proton transfer within the nucleophile. One is the HO^- -S_{N2} pathway; here, HO^- behaves as the attacking nucleophile and generates $\text{CH}_3\text{OH} + \text{H}_2\text{O}_2 + \text{I}^-$, and this reaction occurs at b values of 1, 3, 5, 7, 9, and 11 Å. The other is the HO^- -E2 pathway, which generates the same products as normal

HOO^- -E2, *i.e.*, $\text{C}_2\text{H}_4 + \text{H}_2\text{O}_2 + \text{H}_2\text{O} + \text{I}^-$, but the attacking base is HO^- . This reaction occurs at b values of 0, 1, 3, 7, 9 and 13 Å. However, both pathways are quite rare, where the HO^- -S_{N2} and HO^- -E2 paths account for 2.2% and 2.6%, respectively, of the overall products. At an E_{coll} of 1.0 eV, only the HO^- -E2 pathway is observed, with a minor contribution of 6.8%. Nevertheless, the observation of these HO^- -attacking trajectories highlights the unique role of water molecules in shaping the reaction dynamics.^{32,54}

Furthermore, the solvated products, *i.e.*, $\text{I}^-(\text{H}_2\text{O})$ and $\text{I}^-(\text{HOOH})$, are observed in both the S_{N2} and E2 reaction trajectories. Although the calculated reaction energies are more negative for the solvated products than for the separated products (Fig. S1†), the unsolvated product I^- ions dominate over the solvated $\text{I}^-(\text{solvent})$ ions. In comparison, the reaction energy of the $\text{CH}_3\text{OOH} + \text{I}^-(\text{H}_2\text{O})$ products is $-47.8 \text{ kcal mol}^{-1}$, and this value is $11.4 \text{ kcal mol}^{-1}$ lower than that of the $\text{CH}_3\text{OOH} + \text{I}^- + \text{H}_2\text{O}$ products; the reaction energy of the $\text{C}_2\text{H}_4 + \text{I}^-(\text{H}_2\text{O}) + \text{H}_2\text{O}_2$ products is $-22.7 \text{ kcal mol}^{-1}$, and this value is $11.4 \text{ kcal mol}^{-1}$ lower than that of the $\text{C}_2\text{H}_4 + \text{I}^- + \text{H}_2\text{O} + \text{H}_2\text{O}_2$ products. At an E_{coll} of 0.04 eV, the simulated product anion ratio $\text{I}^- : \text{I}^-(\text{solvent})$ is approximately 97 : 3, highlighting that solvated pathways are suppressed because of the dynamic nature of the reactions in the gas phase; these results are consistent with previous experimental and theoretical works.^{8,22,30,64} When the collision energy is increased to 1.0 eV, no solvated ions are found. Halogen-bonded

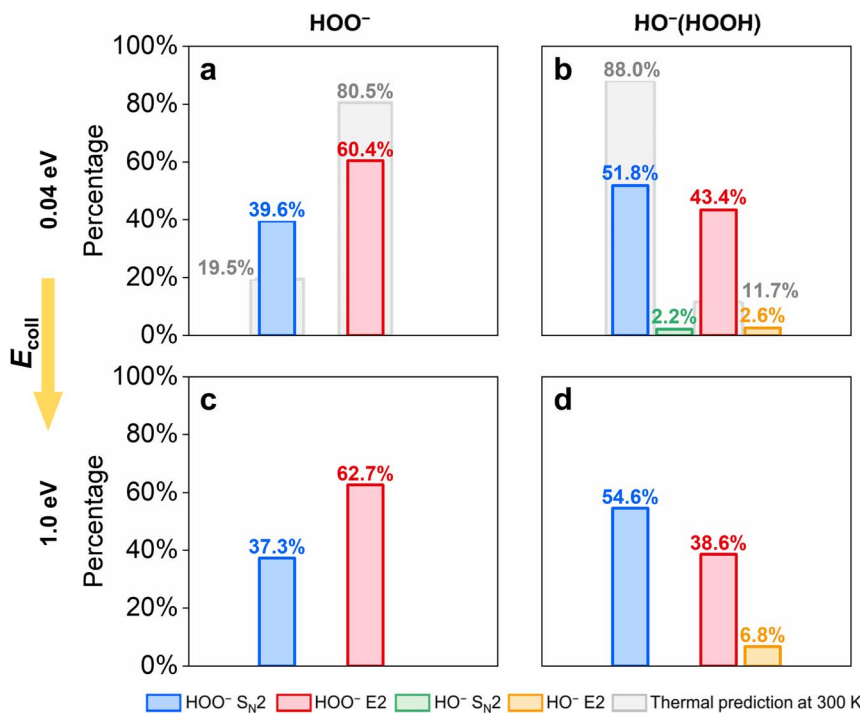


Fig. 2 Branching ratios of the HOO^- - $\text{S}_{\text{N}}2$ (blue), HOO^- - $\text{E}2$ (red), HO^- - $\text{S}_{\text{N}}2$ (green) and HO^- - $\text{E}2$ (orange) pathways for $\text{CH}_3\text{CH}_2\text{I}$ reacting with (a and c) HOO^- and (b and d) HO^- (HOOH) at collision energies of 0.04 eV (top) and 1.0 eV (bottom).

complexes, either $[\text{C}_2\text{H}_5 \cdots \text{I} \cdots \text{OOH}]^-$ or $[\text{C}_2\text{H}_5 \cdots \text{I} \cdots \text{OOH}]^-(\text{H}_2\text{O})$, are observed in both solvent-free and singly solvated systems and are less than 1%.

Moreover, the additional water molecules shift the preference between the $\text{S}_{\text{N}}2$ and $\text{E}2$ pathways compared with the solvent-free case (Fig. 2b and d). For the singly solvated system, at an E_{coll} of 0.04 eV, the HOO^- - $\text{S}_{\text{N}}2$ path has a higher $P_r(b)$ than the HOO^- - $\text{E}2$ path from b of 0 to 5 Å, and they have similar $P_r(b)$ values at b values of 7 to 13 Å. At an E_{coll} of 1.0 eV, the HOO^- - $\text{S}_{\text{N}}2$ path has a higher $P_r(b)$ at b values of 1 and 5 Å. The resulting branching ratios of $\text{E}2 : \text{S}_{\text{N}}2$ are approximately 46 : 54 under both collision energies. Considering only the HOO^- pathways, *i.e.*, excluding the HO^- pathways, $\text{S}_{\text{N}}2$ is also preferred over $\text{E}2$. The phenomenon that solvent molecules promote a portion of the $\text{S}_{\text{N}}2$ path has also been observed in $\text{F}^-(\text{CH}_3\text{OH}) + \text{CH}_3\text{CH}_2\text{Br}$ reactions.^{4,5} Why does a single water molecule shift the preference between the $\text{S}_{\text{N}}2$ and $\text{E}2$ pathways in the studied system? To answer this question, we analysed the potential energy profiles, the atomistic mechanisms and the dynamics of water molecules in the following section.

Potential energy profiles

The potential energy profile of each $\text{S}_{\text{N}}2$ and $\text{E}2$ pathway (Fig. 3) displays a double-well shape, where a central transition state (TS) connects a shallow well of pre-reaction complex (RC) and a deep well of the postreaction complex (PC). All $\text{S}_{\text{N}}2$ and $\text{E}2$ reactions are highly exoergic, and the $\text{S}_{\text{N}}2$ products are more exoergic.

For the unsolvated system, both the back-side $\text{S}_{\text{N}}2$ pathway (denoted as a) and the *anti*- $\text{E}2$ pathway (denoted as c) share the

same pre-reaction complex (denoted as 0aRC), with a relative energy of $-18.3 \text{ kcal mol}^{-1}$ with respect to reactants $\text{HOO}^- + \text{C}_2\text{H}_5\text{I}$. The relative energies of the transition states of the $\text{S}_{\text{N}}2$ pathway (0aTS, $-17.9 \text{ kcal mol}^{-1}$) and the *anti*- $\text{E}2$ pathway (0cTS, $-17.7 \text{ kcal mol}^{-1}$) exceed that of 0aRC by less than 1 kcal mol^{-1} . These results indicate that overcoming both barriers is easy. When the $\text{E}2$ reaction proceeds *via* a *syn*- $\text{E}2$ mechanism, the HOO^- group abstracts the H^β atom from the same side of leaving group I, and its transition state (0c'TS) is much greater in energy, with a value of $-7.4 \text{ kcal mol}^{-1}$ with respect to the reactants. The halogen complex $[\text{C}_2\text{H}_5 \cdots \text{I} \cdots \text{OOH}]^-$ ($-19.0 \text{ kcal mol}^{-1}$) has a similar energy as 0aRC.

One water molecule is added to the HOO^- anion to form HO^- (HOOH), and HO^- (H_2O) is $29.1 \text{ kcal mol}^{-1}$ exoergic. Starting from HO^- (HOOH) + $\text{C}_2\text{H}_5\text{I}$, the reaction energies of the HOO^- - $\text{S}_{\text{N}}2$, HO^- - $\text{S}_{\text{N}}2$, and $\text{E}2$ pathways are -36.4 , -30.0 , and $-11.3 \text{ kcal mol}^{-1}$, respectively. The HOO^- - $\text{S}_{\text{N}}2$ and HOO^- - $\text{E}2$ pathways share the same RC, *i.e.*, 1aRC, and the HO^- - $\text{S}_{\text{N}}2$ (denoted as b) and HO^- - $\text{E}2$ pathways (denoted as d) share the same RC, denoted as 1bRC. The nomenclatures of TS and PC use the a, b, c, and d annotations. The pre-reaction complex for the HO^- path (1bRC, $-14.3 \text{ kcal mol}^{-1}$) is slightly more stable than that for the HOO^- path (1aRC, $-13.0 \text{ kcal mol}^{-1}$), as observed for the reaction with $\text{CH}_3\text{Cl}/\text{CH}_3\text{I}$.^{32,54} Nevertheless, the transition states of the HO^- paths are higher in energy than that for the HOO^- path (either the $\text{S}_{\text{N}}2$ path or the $\text{E}2$ path). Arranged in ascending order of transition state energies, the order of pathways is HOO^- - $\text{S}_{\text{N}}2 < \text{HO}^-$ - $\text{S}_{\text{N}}2 < \text{HOO}^-$ - $\text{E}2$ (*anti*) $< \text{HO}^-$ - $\text{E}2$ (*anti*). The energies are -9.4 , -7.1 , -6.2 , and $-4.0 \text{ kcal mol}^{-1}$ for 1aTS, 1bTS, 1cTS, and 1dTS, respectively.

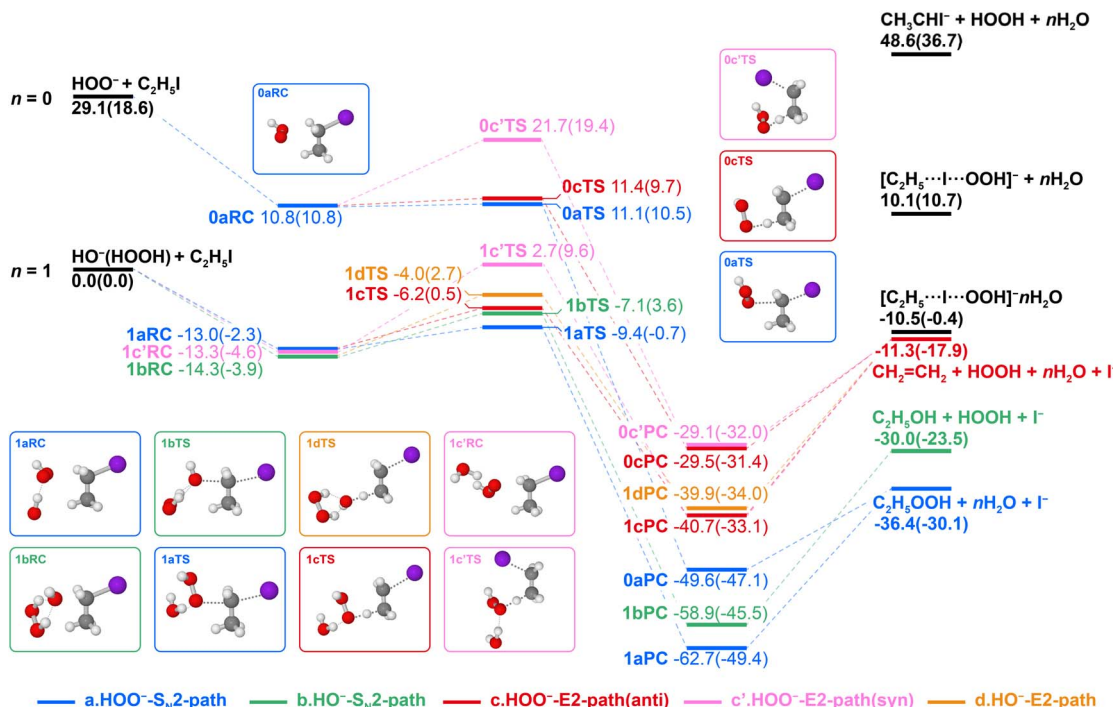


Fig. 3 Potential energy profile of $\text{CH}_3\text{CH}_2\text{I}$ reacting with HOO^- and $\text{HO}^-(\text{HOOH})$. (a) refers to the backside attack HOO^- - $\text{S}_{\text{N}}2$ pathway (blue); (b) refers to the backside attack HO^- - $\text{S}_{\text{N}}2$ pathway (green); (c) refers to the antisymmetric HOO^- -E2 pathway (red); (c') refers to the *syn*-symmetric HOO^- -E2 pathway (orange). Energy values (in kcal mol^{-1}) excluding zero-point energy corrections are in normal text, and the values of Gibbs free energy at 298.15 K are in parentheses.

When the free energies are compared, the transition state of HO^- - $\text{S}_{\text{N}}2$ has the highest free energy among these four TSs. As expected, the *syn*-E2 path has an even higher transition state, $1\text{c}'\text{TS}$, whose relative energy is $2.7 \text{ kcal mol}^{-1}$ in electronic energy and $9.6 \text{ kcal mol}^{-1}$ in free energy.

Assuming a Boltzmann distribution of these four pathways and according to the calculated free energies of the TSs, the thermal ratio at 300 K of HOO^- - $\text{S}_{\text{N}}2$: HOO^- -E2 is $19.5 : 80.5$ for the unsolvated system, and the thermal ratio of HOO^- - $\text{S}_{\text{N}}2$: HO^- - $\text{S}_{\text{N}}2$: HOO^- -E2 : HO^- -E2 is $87.9 : 0.1 : 11.7 : 0.3$ for the singly solvated system. At an E_{coll} of 0.04 eV , corresponding to a temperature of 300 K , the ratios given by direct dynamic simulations are $39.6 : 60.4$ and $51.8 : 2.2 : 43.4 : 2.6$. The thermal distribution predictions (based on stationary point calculations) and dynamic simulation results are consistent in that the HOO^- -E2 path is dominant under unsolvated conditions, whereas the HOO^- - $\text{S}_{\text{N}}2$ path is dominant under singly solvated conditions. Notably, the simulations provide a much higher percentage of the HOO^- -E2 path, differing by $20\text{--}30\%$, and a slightly higher percentage of the HO^- paths. These results highlighted the dynamic characteristics of the reaction process. The dynamic preference of the E2 product channel has also been observed in the $\text{F}^-(\text{CH}_3\text{OH}) + \text{C}_2\text{H}_5\text{Br}$ reaction,^{4,5} where the dominant pathway given by simulation becomes the E2 path instead of the $\text{S}_{\text{N}}2$ path, which was predicted by the thermal distribution. The atomistic mechanisms discussed in the next section provide a detailed picture of the dynamic characteristics.

Atomistic mechanisms

Different types of mechanisms were observed by tracking the animations of each reactive trajectory. The distribution of the mechanisms is shown in Fig. 4. The mechanisms are classified into direct and indirect mechanisms, depending on whether intermediates are formed during the trajectory.^{20,65} For the unsolvated system, the reaction mechanism is primarily direct. At an E_{coll} of 0.04 eV , the direct HOO^- - $\text{S}_{\text{N}}2$ mechanism accounts for 24.2% , and the direct HOO^- -E2 mechanism accounts for 40.4% ; at an E_{coll} of 1.0 eV , the corresponding values are 34.2% and 57.8% , respectively. As expected, a higher collision energy leads to more direct trajectories. For both the HOO^- - $\text{S}_{\text{N}}2$ and E2 pathways, both direct stripping (DS) and direct rebound (DR) mechanisms were observed, where the former is more common. The features of these mechanisms have been described in previous works,^{20,65,66} and representative animations are presented in the ESI Movies.† The addition of one water molecule increases the percentage of indirect mechanisms. For the singly hydrated system, at an E_{coll} of 0.04 eV , the indirect HOO^- - $\text{S}_{\text{N}}2$ mechanism accounts for 40.5% , and the indirect HOO^- -E2 mechanism accounts for 29.8% ; at an E_{coll} of 1.0 eV , the corresponding values are 22.2% and 21.8% , respectively. These values are much higher than the corresponding values from the unsolvated system, which are 15.4 , 20.0 , 3.1 , and 4.9% (Fig. 4). The distributions of the product I^- ion velocity scattering angle are shown in Fig. S2,† where the indirect mechanism shows isotropic scattering.

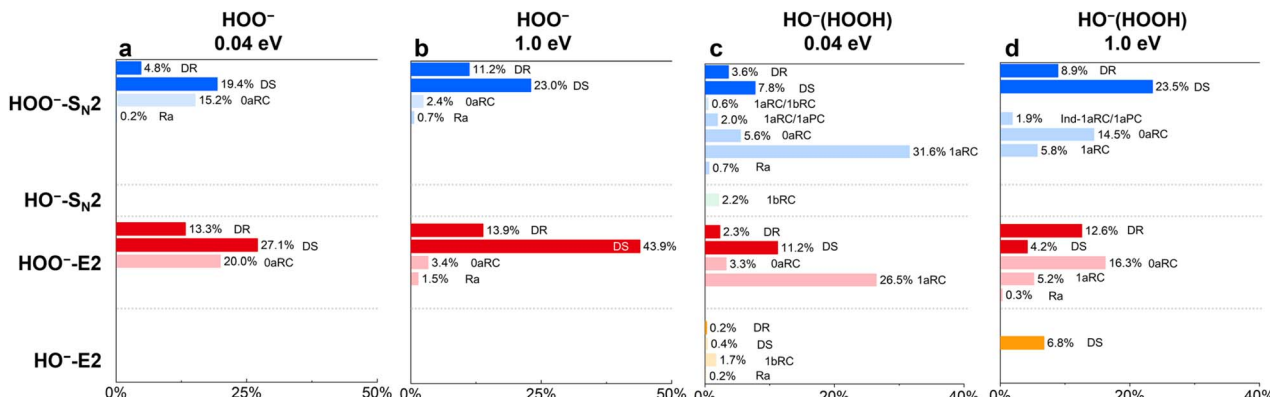


Fig. 4 Distributions of the reaction mechanisms for the S_N2 and E2 pathways for CH_3CH_2I reacting with (a and b) HOO^- and (c and d) $HO^-(HOOH)$ at collision energies of 0.04 and 1.0 eV. Note: For unsolvated systems, the 0aRC mechanism involves α -elimination and H^α -exchange mechanisms.

For both unsolvated and singly solvated systems, the observed indirect mechanisms include the formation of various intermediates and roundabout (Ra) mechanisms, where the latter contribute less than 3%. Previous reports of roundabout mechanisms of E2 reactions were limited to F^- nucleophiles;^{5,56,67,68} this work extends the roundabout mechanism to HOO^- and $HO^-(HOOH)$ reactions.

For both the S_N2 and E2 pathways, the dominant indirect mechanism is the formation of the $HOO^- \cdots C_2H_5I$ complex (0aRC) for the unsolvated system at both E_{coll} values and the singly solvated system at an E_{coll} of 1.0 eV. The dominant indirect mechanism becomes the formation of the $(H_2O)HOO^- \cdots C_2H_5I$ complex (1aRC) for the singly solvated system at an E_{coll} of 0.04 eV. In addition, the mechanism of the singly solvated system was complicated by the participation of multiple intermediates, including 0aRC, 1aRC, 1bRC, and 1aPC. To demonstrate the indirect mechanisms, we provide snapshots of representative trajectories in Fig. 5. Fig. 5a shows an indirect $HOO^- \cdots S_N2$ trajectory that is trapped in the pre-reaction complex 1aRC well for approximately 4 ps before the products are formed. Fig. 5c displays an indirect $HOO^- \cdots E2$ trajectory that is trapped in the 1aRC well for ~ 9 ps. Then, the $HOO^- (H_2O)$ group abstracts the H^β atom from the opposite side of leaving group I; specifically the *anti*-E2 mechanism occurs, and E2 products are formed. The lifetimes of pre-reaction complexes 1aRC were analysed by plotting $\ln[N(t)/N(0)]$ versus time (t) for the trajectories, where $N(0)$ refers to the number of trajectories that experienced the formation of RCs and $N(t)$ refers to the number of trajectories whose lifetimes of RCs are no less than t (Fig. S3†). The resulting dissociation rate constant of 1aRC is 0.13 ps^{-1} for the S_N2 path and 0.16 ps^{-1} for the E2 path. Consequently, the corresponding half-lives of 1aRC are 5.33 and 4.33 ps; these results indicate that the reaction system was trapped in the pre-reaction complex well.

In addition to the *anti*-E2 mechanism, we also observed trajectories that follow the *syn*-E2 mechanism (Fig. S4b†). Owing to the higher transition states (Fig. 3) and greater steric hindrance than those of the *anti*-E2 paths, the *syn*-E2 trajectories constitute only a small portion of all E2 trajectories. For the

unsolvated system, the fraction of *syn*-E2 trajectories is approximately 3% and 8% at E_{coll} values of 0.04 and 1.0 eV; for the singly solvated system, the corresponding fractions are 0.9% and 0.

In the abovementioned *anti*-E2 and *syn*-E2 trajectories, the nucleophile first abstracts H^β from the substrate CH_3CH_2I . For the unsolvated system at an E_{coll} of 1.0 eV, the E2 trajectories may be initiated by a nucleophile abstracting a H^α atom. As shown in Fig. S5b,† HOO^- initially abstracts an H^α atom from the CH_3CH_2I substrate to form $HOOH$, followed by the C–I bond breaking, and then the substrate becomes CH_3CH . Thereafter, the substrate goes through an H^β -transfer transition state (E α TS) to generate $CH_2=CH_2$. This mechanism is called α -elimination (E α) in previous simulations of $F^- + CH_3CH_2Br$ reactions,⁵ and this name is adopted here. The barrier of E α TS is as high as 7.9 kcal mol⁻¹ (Fig. S6†); thus, this mechanism is highly unfavourable and is observed only at an E_{coll} of 1.0 eV and accounts for 2.2% of the $HOO^- \cdots E2$ path.

In addition, the trajectories that experience the formation of 0aRC sometimes involve hydrogen exchange (HE) between the nucleophile HOO^- and substrates, as observed in both the S_N2 and E2 pathways (Fig. S5b and S5c†). Similar to the first step of the E α mechanism, the nucleophile initially abstracts an H^α atom from the CH_3CH_2I substrate. The newly formed $HOOH$ moiety transfers an H atom to C^α simultaneously or after a period, and then, the system reforms the CH_3CH_2I and HOO^- parts. This H-atom can be either the same H^α or the H that originally belonged to the nucleophile HOO^- . For the latter case, a transition state was located with a high barrier of 9.5 kcal mol⁻¹. Proton exchange may occur several times within a trajectory. These multiple types of hydrogen exchange trajectories are presented in Fig. S5 and S7.† Overall, these trajectories account for 0.36% (2.17%) of the S_N2 reactions and 0.63% (0.12%) of the E2 reactions at an E_{coll} of 0.04 eV (1.0 eV). Notably, the H^α -abstraction may generate $CH_3CHI^- + HOOH$ products. The product channel is 48.6 endothermic and was not observed during our simulation. However, a trace amount of $CH_3CH_2Cl^-$ was observed in previous simulations of $F^-/HO^- + CH_3CH_2Cl$.^{69,70}



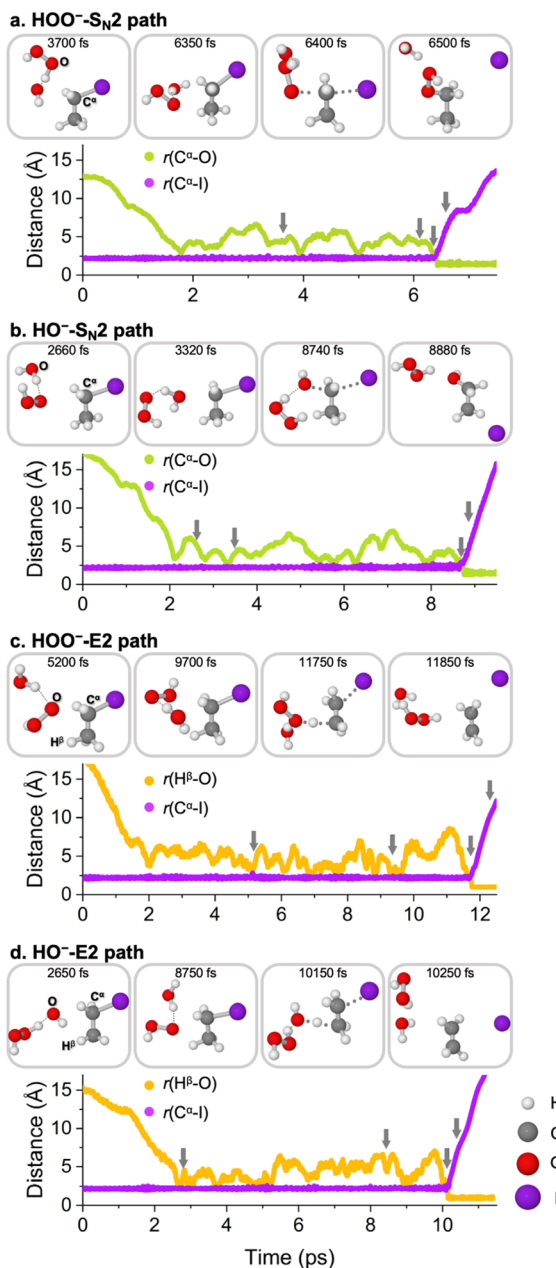


Fig. 5 Snapshots of the representative trajectories showing the indirect mechanism of the $\text{HOO}^-(\text{H}_2\text{O}) + \text{CH}_3\text{CH}_2\text{I}$ reaction. The distance between the C^α atom and I atom $r(\text{C}^\alpha\text{-I})$ (purple), the distance between the C^α atom and the attacking O atom $r(\text{C}^\alpha\text{-O})$ (green), and the distance between H^β and the attacking O atom $r(\text{H}^\beta\text{-O})$ (orange) are shown as a function of time. (a) $\text{HOO}^-\text{-S}_{\text{N}2}$ pathway, (b) $\text{HO}^-\text{-S}_{\text{N}2}$ pathway, (c) $\text{HOO}^-\text{-E}2$ pathway, (d) $\text{HO}^-\text{-E}2$ pathway.

Interestingly, these α -elimination and H^α -exchange mechanisms were not observed in the singly hydrated system. This can be understood by comparing the proton affinities (PAs). The PA of HOO^- is 375.9 kcal mol⁻¹, and the PA of $\text{HO}^-(\text{HOOH})$ is 357.0 kcal mol⁻¹; thus, the abstraction of either H^α or H^β from $\text{CH}_3\text{CH}_2\text{I}$ by $\text{HO}^-(\text{HOOH})$ is more difficult than that by HOO^- . Instead, the proton transfer between the nucleophiles and substrates is completely suppressed by proton transfer within

the singly solvated nucleophile $\text{HO}^-(\text{HOOH})$. Representative trajectory snapshots are shown in Fig. S8 and S9.[†]

For the water-induced $\text{HO}^-\text{-S}_{\text{N}2}$ and $\text{HO}^-\text{-E}2$ pathways, Fig. 5b and d show that these trajectories also experience a long time (approximately 6–7 ps) within the pre-reaction complex well; here, the nucleophile group strongly interconverts between $\text{HOO}^-(\text{H}_2\text{O})$ and $\text{HO}^-(\text{HOOH})$. The singly solvated pre-reaction complexes $(\text{H}_2\text{O})\text{HOO}^-\cdots\text{C}_2\text{H}_5\text{I}$ (1aRC) and $(\text{HOOH})\text{HO}^-\cdots\text{C}_2\text{H}_5\text{I}$ (1bRC) are close in energy, and the latter is approximately 1 kcal mol⁻¹ more stable. However, tracking the trajectories within the well indicates that the system prefers to stay in the configuration of $(\text{H}_2\text{O})\text{HOO}^-\cdots\text{C}_2\text{H}_5\text{I}$. For example, for a representative $\text{HO}^-\text{-S}_{\text{N}2}$ trajectory (Fig. 5b) and considering the time within the pre-reaction complex well, the system adopts the $(\text{H}_2\text{O})\text{HOO}^-\cdots\text{C}_2\text{H}_5\text{I}$ configuration 69% of the time, and this value is 73% for a representative $\text{HO}^-\text{-E}2$ trajectory (Fig. 5d). The more stable $(\text{HOOH})\text{HO}^-\cdots\text{C}_2\text{H}_5\text{I}$ configuration only accounts for 31% and 27%, respectively. A detailed analysis is provided in Fig. S10.[†] This occurs because the symmetric structure of $(\text{HOOH})\text{HO}^-$ in 1bRC can easily be disturbed during the dynamic reaction process, namely, the entropy effect. Hence, the lower probability of the HO^- configurations within the well and the higher barrier both lead to the suppression of the HO^- paths, both $\text{S}_{\text{N}2}$ and $\text{E}2$. Nevertheless, the simulated HO^- paths have a slightly greater portion than those predicted by the thermal distribution at 300 K; these results indicate the dynamic effects of proton transfer during the reaction processes.

Finally, we investigated the reason for the suppression of the thermodynamically favoured solvated product I^- (solvent) by the I^- product from the simulation. To understand this, we plotted the time at which the H_2O molecule departed from the system against the formation time of $\text{CH}_3\text{CH}_2\text{OOH}$ for the $\text{HOO}^-\text{-S}_{\text{N}2}$ pathway and against the formation time of $\text{CH}_2=\text{CH}_2$ for the $\text{HOO}^-\text{-E}2$ pathway (Fig. 6). At $E_{\text{coll}} = 0.04$ eV, the formation of

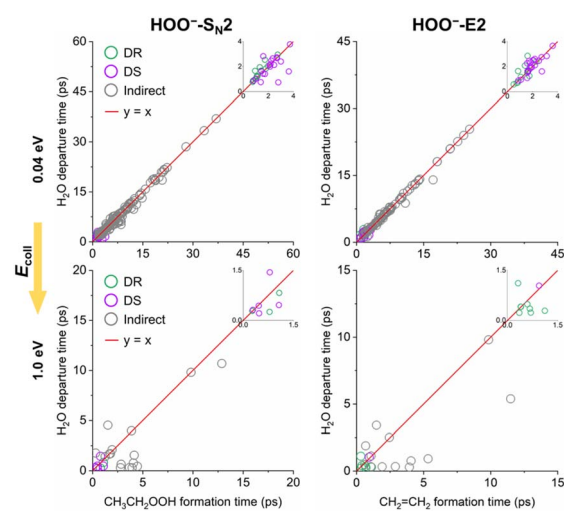


Fig. 6 Water-leaving time as a function of $\text{CH}_3\text{CH}_2\text{OOH}$ (left) and $\text{CH}_2=\text{CH}_2$ (right) formation time for the $\text{HOO}^-(\text{H}_2\text{O}) + \text{CH}_3\text{CH}_2\text{I}$ reaction at 0.04 (top) and 1.0 eV (bottom) collision energies.



$\text{CH}_3\text{CH}_2\text{OOH}$ or $\text{CH}_2=\text{CH}_2$ simultaneously occurred with the departure of H_2O , mostly within 20 ps. As E_{coll} increased to 1.0 eV, the majority of $\text{S}_{\text{N}2}$ reactions occurred within 5 ps, whereas the H_2O molecules were removed much earlier, mainly before 2.5 ps. Similarly, the E2 reactions occurred within \sim 4 ps, and the H_2O molecules were removed before 2.0 ps. With a time width of \pm 250 fs centred on the unit slope line, the percentages of the trajectories for $\text{S}_{\text{N}2}$ and E2 were 65.2% and 71.5%, respectively, at $E_{\text{coll}} = 0.04$ eV, and the corresponding values decreased to 46.0% and 41.4%, respectively, at $E_{\text{coll}} = 1.0$ eV. The above analysis, together with the mechanism analysis, indicated that a large portion of the collision energy and/or the reaction exothermicity were transferred to the relative translational energy of the solvent and the remaining parts. Consequently, solvated products were rarely observed.

Conclusions

In this work, the effect of a single water molecule on the reaction between the hydroperoxide anion and ethyl iodide was investigated by direct dynamics simulation. The introduction of one water molecule had multiple effects. First, it lowered the overall reactivity; here, the rate constant was reduced by 61% and 63% in comparison to that of the solvent-free reaction, under the considered collision energies of 0.04 and 1.0 eV. Second, it changed the preference between the competing $\text{S}_{\text{N}2}$ and E2 reactions. The $\text{S}_{\text{N}2}$ -to-E2 ratio was approximately 40 : 60 for the solvent-free system, and this ratio changed to approximately 54 : 46 for the single-solvation system under both E_{coll} values. A single solvent shifted the preference from E2 to $\text{S}_{\text{N}2}$ because of the differential solvation effect that led to a higher barrier for the E2 path than for the $\text{S}_{\text{N}2}$ path. However, the dynamical simulations resulted in more E2 trajectories than what was predicted by the potential energy profiles. Increasing E_{coll} did not affect the $\text{S}_{\text{N}2}$ -to-E2 ratio but lowered the overall reactivity by 82%.

Third, the extra water molecules facilitated new pathways *via* proton transfer between $\text{HOO}^-(\text{H}_2\text{O})$ and $\text{HO}^-(\text{HOOH})$, thus leading to the $\text{HO}^-\text{S}_{\text{N}2}$ and $\text{HO}^-\text{E2}$ paths, in addition to the traditional $\text{HOO}^-\text{S}_{\text{N}2}$ and $\text{HOO}^-\text{E2}$ paths, where the latter two paths were dominant. The percentages of $\text{HOO}^-\text{S}_{\text{N}2}$, $\text{HOO}^-\text{E2}$, $\text{HO}^-\text{S}_{\text{N}2}$, and $\text{HO}^-\text{E2}$ paths were 51.8%, 43.4%, 2.2%, and 2.6%, respectively, at an E_{coll} of 0.04 eV and 54.6%, 38.6%, 0, and 6.8%, respectively, at an E_{coll} of 1.0 eV. Extensive proton transfer within the pre-reaction complex well drove the occurrence of the HO^- paths. However, the lower probability of HO^- configurations that caused by the entropy effect and the relatively higher barrier led to their low percentages. We anticipate that the solvent molecule inducing new pathways is not an isolated case, especially for protic solvents such as H_2O , NH_3 , and CH_3OH . However, such studies are quite limited so far. Singly-solvated anions like $\text{OH}^-(\text{H}_2\text{O})$, $\text{NH}_2^-(\text{NH}_3)$, and $\text{CH}_3\text{O}^-(\text{CH}_3\text{OH})$ experience extensive proton exchange, but generate the same type of anions. Anions like $\text{F}^-(\text{H}_2\text{O})$, $\text{HO}^-(\text{NH}_3)$, $\text{HOO}^-(\text{NH}_3)$, and $\text{CH}_3\text{O}^-(\text{H}_2\text{O})$ can generate new nucleophiles through proton transfer, but they are usually higher in energy. Their dynamics remain to be explored in the future.

Fourth, the introduction of one water molecule complicated the reaction mechanisms, increased the percentage of indirect mechanism, and affected the dynamical feature of proton transfer. For the solvent-free system, proton transfer occurred between nucleophiles and substrates; for example, α -elimination and H^{α} -exchange mechanisms were observed. In contrast, for the singly solvated system, proton transfer mainly occurred within the nucleophile, *i.e.*, the configurations shifted between $(\text{H}_2\text{O})\text{HOO}^-\cdots\text{C}_2\text{H}_5\text{I}$ and $(\text{HOOH})\text{HO}^-\cdots\text{C}_2\text{H}_5\text{I}$. Finally, solvated products were observed for the singly solvated reactions, but at a very low percentage of 3%. This occurred because a large portion of the collision energy and/or the reaction exothermicity were transferred to the translation of the products.

To conclude, this work revealed that for the $\text{HOO}^- + \text{C}_2\text{H}_5\text{I}$ reaction, a single water molecule affected more than the reactivity and competition between the $\text{S}_{\text{N}2}$ and E2 reactions. It also induced new competing pathways that used HO^- as an attacking nucleophile *via* proton transfer and complicated the reaction mechanisms. These dynamic roles of the individual solvent molecules observed in this work could reveal new facets of reaction dynamics relevant to organic synthesis, biochemistry,^{71,72} microdroplet chemistry,⁷³⁻⁷⁶ and chemistry in aerosols.⁷⁷⁻⁸⁰

Data availability

Data are in ESI.†

Author contributions

J. X. designed the research. X. Wu performed the computations, analyzed the data, prepared the figures and tables, and wrote the draft of the paper. C. Z. edited the paper. J. X. and J. S. F. supervised the research and edited the paper.

Conflicts of interest

There are no conflicts to declare.

Acknowledgements

This work was supported by the National Key Research and Development Program of China (2024YFA1509602), the National Natural Science Foundation of China (no. 22273004), and the Teli Fellowship and the Innovation Foundation (no. 2021CX01026) from the Beijing Institute of Technology, China.

References

- 1 E. Vöhringer-Martinez, B. Hansmann, H. Hernandez, J. S. Francisco, J. Troe and B. Abel, *Science*, 2007, **315**, 497–501.
- 2 G. I. Almerindo and J. R. Pliego, *Chem. Phys. Lett.*, 2006, **423**, 459–462.
- 3 X. Liu, J. Xie, J. Zhang, L. Yang and W. L. Hase, *J. Phys. Chem. Lett.*, 2017, **8**, 1885–1892.



4 X. Liu, J. Zhang, L. Yang and W. L. Hase, *J. Am. Chem. Soc.*, 2018, **140**, 10995–11005.

5 H. Wang, X. Liu, S. Zhao, G. Fu, W. Zhen, L. Yang and J. Zhang, *Precis. Chem.*, 2024, **2**, 40–48.

6 D. K. Bohme and G. I. Mackay, *J. Am. Chem. Soc.*, 1981, **103**, 978–979.

7 F. M. Bickelhaupt, E. J. Baerends and N. M. M. Nibbering, *Chem.-Eur. J.*, 1996, **2**, 196–207.

8 N. Eyet, J. J. Melko, S. G. Ard and A. A. Viggiano, *Int. J. Mass Spectrom.*, 2015, **378**, 54–58.

9 T. Hansen, J. C. Roozee, F. M. Bickelhaupt and T. A. Hamlin, *J. Org. Chem.*, 2022, **87**, 1805–1813.

10 R. Otto, J. Brox, S. Trippel, M. Stei, T. Best and R. Wester, *Nat. Chem.*, 2012, **4**, 534–538.

11 L. Yang, X. Liu, J. Zhang and J. Xie, *Phys. Chem. Chem. Phys.*, 2017, **19**, 9992–9999.

12 K. Doi, E. Togano, S. S. Xantheas, R. Nakanishi, T. Nagata, T. Ebata and Y. Inokuchi, *Angew. Chem., Int. Ed.*, 2013, **52**, 4380–4383.

13 C. Zhu, X. C. Zeng, J. S. Francisco and I. Gladich, *J. Am. Chem. Soc.*, 2020, **142**, 5574–5582.

14 B. Tang, Q. Bai, Y.-G. Fang, J. S. Francisco, C. Zhu and W.-H. Fang, *J. Am. Chem. Soc.*, 2024, **146**, 21742–21751.

15 Y.-G. Fang, L. Wei, J. S. Francisco, C. Zhu and W.-H. Fang, *J. Am. Chem. Soc.*, 2024, **146**, 21052–21060.

16 Z. Wan, C. Zhu and J. S. Francisco, *J. Am. Chem. Soc.*, 2023, **145**, 17478–17484.

17 Z. Wan, Y. Fang, Z. Liu, J. S. Francisco and C. Zhu, *J. Am. Chem. Soc.*, 2023, **145**, 944–952.

18 G. T. Dunning, D. R. Glowacki, T. J. Preston, S. J. Greaves, G. M. Greetham, I. P. Clark, M. Towrie, J. N. Harvey and A. J. Orr-Ewing, *Science*, 2015, **347**, 530–533.

19 F. Xie, D. S. Tikhonov and M. Schnell, *Science*, 2024, **384**, 1435–1440.

20 J. Xie, R. Otto, J. Mikosch, J. Zhang, R. Wester and W. L. Hase, *Acc. Chem. Res.*, 2014, **47**, 2960–2969.

21 R. Otto, J. Xie, J. Brox, S. Trippel, M. Stei, T. Best, M. R. Siebert, W. L. Hase and R. Wester, *Faraday Discuss.*, 2012, **157**, 41–57.

22 R. Otto, J. Brox, S. Trippel, M. Stei, T. Best and R. Wester, *J. Phys. Chem. A*, 2013, **117**, 8139–8144.

23 B. Bastian, T. Michaelsen, L. Li, M. Ončák, J. Meyer, D. H. Zhang and R. Wester, *J. Phys. Chem. A*, 2020, **124**, 1929–1939.

24 B. Bastian, T. Michaelsen, M. Ončák, J. Meyer and R. Wester, *Int. J. Mass Spectrom.*, 2021, **462**, 116526.

25 X. Lu, L. Li, X. Zhang, B. Fu, X. Xu and D. H. Zhang, *J. Phys. Chem. Lett.*, 2022, **13**, 5253–5259.

26 X. Lu, C. Shang, L. Li, R. Chen, B. Fu, X. Xu and D. H. Zhang, *Nat. Commun.*, 2022, **13**, 4427.

27 D. A. Tasi and G. Czakó, *Chem. Sci.*, 2021, **12**, 14369–14375.

28 Y. Feng, L. Zhou, Q. Wan, S. Lin and H. Guo, *Chem. Sci.*, 2018, **9**, 5890–5896.

29 R. Yin, B. Jiang and H. Guo, *ACS Catal.*, 2022, **12**, 6486–6494.

30 J. Xie, R. Otto, R. Wester and W. L. Hase, *J. Chem. Phys.*, 2015, **142**, 244308.

31 J. Xie, X. Ma, J. Zhang, P. M. Hierl, A. A. Viggiano and W. L. Hase, *Int. J. Mass Spectrom.*, 2017, **418**, 122–129.

32 C. Zhao, X. Ma, X. Wu, D. L. Thomsen, V. M. Bierbaum and J. Xie, *J. Phys. Chem. Lett.*, 2021, **12**, 7134–7139.

33 M. A. Vincent, I. J. Palmer, I. H. Hillier and E. Akhmatkaya, *J. Am. Chem. Soc.*, 1998, **120**, 3431–3439.

34 J. A. Cotruvo, Jr. and J. Stubbe, *Biochemistry*, 2010, **49**, 1297–1309.

35 L. Q. Tuan, H. Umakoshi, T. Shimanouchi and R. Kuboi, *Enzyme Microb. Technol.*, 2009, **44**, 101–106.

36 M. A. Babizhayev, K. S. Vishnyakova and Y. E. Yegorov, *Fundam. Clin. Pharmacol.*, 2011, **25**, 139–162.

37 L. Qiao, Y. Lu, B. Liu and H. H. Girault, *J. Am. Chem. Soc.*, 2011, **133**, 19823–19831.

38 H. Wang, Z. Song, W. Liu and H. Kong, *Microelectron. Eng.*, 2011, **88**, 1010–1015.

39 S. Siddiqui, M. Keswani, B. Brooks, A. Fuerst and S. Raghavan, *Microelectron. Eng.*, 2013, **102**, 68–73.

40 S. H. Zeronian and M. K. Inglesby, *Cellulose*, 1995, **2**, 265–272.

41 S. W. Benson and P. S. Nangia, *Acc. Chem. Res.*, 1979, **12**, 223–228.

42 A. B. Fialkov, *Prog. Energy Combust. Sci.*, 1997, **23**, 399–528.

43 Y. Qiao, S. Wu, J. Yi, Y. Sun, S. Guo, S. Yang, P. He and H. Zhou, *Angew. Chem., Int. Ed.*, 2017, **56**, 4960–4964.

44 Z. Ma, D. Anick and M. E. Tuckerman, *J. Phys. Chem. B*, 2014, **118**, 7937–7945.

45 D. L. Thomsen, J. N. Reece, C. M. Nichols, S. Hammerum and V. M. Bierbaum, *J. Am. Chem. Soc.*, 2013, **135**, 15508–15514.

46 D. L. Thomsen, C. M. Nichols, J. N. Reece, S. Hammerum and V. M. Bierbaum, *J. Am. Soc. Mass Spectrom.*, 2014, **25**, 159–168.

47 D. L. Thomsen, J. N. Reece, C. M. Nichols, S. Hammerum and V. M. Bierbaum, *J. Phys. Chem. A*, 2014, **118**, 8060–8066.

48 D. J. Anick, *J. Phys. Chem. A*, 2011, **115**, 6327–6338.

49 F. Yu, *J. Chem. Phys.*, 2018, **148**, 014302.

50 Z. Kerekes, D. A. Tasi and G. Czakó, *J. Phys. Chem. A*, 2022, **126**, 889–900.

51 A. Gutal and M. Paranjothy, *Phys. Chem. Chem. Phys.*, 2023, **25**, 15015–15022.

52 X. Liu, S. Tian, B. Pang, H. Li and Y. Wu, *Phys. Chem. Chem. Phys.*, 2023, **25**, 14812–14821.

53 X. Liu, W. Guo, H. Feng, B. Pang and Y. Wu, *J. Phys. Chem. A*, 2023, **127**, 7373–7382.

54 X. Wu, C. Zhao, S. Zhang and J. Xie, *J. Phys. Chem. A*, 2024, **128**, 2393–2398.

55 X. Wu, C. Zhao and J. Xie, *ChemPhysChem*, 2022, **23**, e202200285.

56 E. Carrascosa, J. Meyer, J. Zhang, M. Stei, T. Michaelsen, W. L. Hase, L. Yang and R. Wester, *Nat. Commun.*, 2017, **8**, 25.

57 L. Yang, J. Zhang, J. Xie, X. Ma, L. Zhang, C. Zhao and W. L. Hase, *J. Phys. Chem. A*, 2017, **121**, 1078–1085.

58 X. Wu, S. Zhang and J. Xie, *Phys. Chem. Chem. Phys.*, 2022, **24**, 12993–13005.



59 X. Wu, F. M. Bickelhaupt and J. Xie, *Phys. Chem. Chem. Phys.*, 2024, **26**, 11320–11330.

60 W. L. Hase, R. J. Duchovic, X. Hu, A. Komornicki, K. F. Lim, D. H. Lu, G. H. Peslherbe, K. N. Swamy, S. R. V. Linde, A. J. C. Varandas, H. Wang and R. J. Wolf, *Quantum Chem. Program Exch. Bull.*, 1996, **16**, 671.

61 M. Valiev, E. J. Bylaska, N. Govind, K. Kowalski, T. P. Straatsma, H. J. J. Van Dam, D. Wang, J. Nieplocha, E. Apra, T. L. Windus and W. A. de Jong, *Comput. Phys. Commun.*, 2010, **181**, 1477–1489.

62 U. Lourderaj, R. Sun, S. C. Kohale, G. L. Barnes, W. A. de Jong, T. L. Windus and W. L. Hase, *Comput. Phys. Commun.*, 2014, **185**, 1074–1080.

63 L. Verlet, *Phys. Rev.*, 1967, **159**, 98–103.

64 J. Zhang, L. Yang, J. Xie and W. L. Hase, *J. Phys. Chem. Lett.*, 2016, **7**, 660–665.

65 J. Xie and W. L. Hase, *Science*, 2016, **352**, 32–33.

66 J. Zhang, J. Mikosch, S. Trippel, R. Otto, M. Weidemüller, R. Wester and W. L. Hase, *J. Phys. Chem. Lett.*, 2010, **1**, 2747–2752.

67 S. Zhao, H. Wang, G. Fu, W. Zhen, M. Liu, L. Yang and J. Zhang, *Precis. Chem.*, 2023, **1**, 507–515.

68 X. Wu, F. Ying, H. Wang, L. Yang, J. Zhang and J. Xie, *ACS Phys. Chem. Au*, 2024, **4**, 581–592.

69 J. Meyer, V. Tajti, E. Carrascosa, T. Györi, M. Stei, T. Michaelsen, B. Bastian, G. Czakó and R. Wester, *Nat. Chem.*, 2021, **13**, 977–981.

70 A. B. Naesa, C. Tokaji and G. Czakó, *Faraday Discuss.*, 2024, **251**, 604–621.

71 D. R. B. Brittain, R. Pandey, K. Kumari, P. Sharma, G. Pandey, R. Lal, M. L. Coote, J. G. Oakeshott and C. J. Jackson, *Chem. Commun.*, 2011, **47**, 976–978.

72 D. O'Hagan and J. W. Schmidberger, *Nat. Prod. Rep.*, 2010, **27**, 900–918.

73 X. Yan, R. M. Bain and R. G. Cooks, *Angew. Chem., Int. Ed.*, 2016, **55**, 12960–12972.

74 S. Banerjee, E. Gnanamani, X. Yan and R. N. Zare, *Analyst*, 2017, **142**, 1399–1402.

75 K. Li, K. Gong, J. Liu, L. Ohnoutek, J. Ao, Y. Liu, X. Chen, G. Xu, X. Ruan, H. Cheng, J. Han, G. Sui, M. Ji, V. K. Valev and L. Zhang, *Cell Rep. Phys. Sci.*, 2022, **3**, 100917.

76 S. Jin, H. Chen, X. Yuan, D. Xing, R. Wang, L. Zhao, D. Zhang, C. Gong, C. Zhu, X. Gao, Y. Chen and X. Zhang, *JACS Au*, 2023, **3**, 1563–1571.

77 J. Li, N. T. Tsiona and L. Du, *Phys. Chem. Chem. Phys.*, 2018, **20**, 10650–10659.

78 N. Tsiona Tchinda, L. Du, L. Liu and X. Zhang, *Atmos. Chem. Phys.*, 2022, **22**, 1951–1963.

79 Y. Liu, Q. Ge, T. Wang, R. Zhang, K. Li, K. Gong, L. Xie, W. Wang, L. Wang, W. You, X. Ruan, Z. Shi, J. Han, R. Wang, H. Fu, J. Chen, C. K. Chan and L. Zhang, *Chem.*, 2024, **10**, 330–351.

80 J. Liu, Y. Zhao, X. Lian, D. Li, X. Zhang, J. Chen, B. Deng, X. Lan and Y. Shao, *Molecules*, 2024, **29**, 4033.

